



# Mixed Electric and Magnetic Coupling Design Based on Coupling Matrix Extraction

XIONG Zhiang<sup>1</sup>, ZHAO Ping<sup>1</sup>, FAN Jiyuan<sup>1</sup>,  
WU Zengqiang<sup>2</sup>, GONG Hongwei<sup>2</sup>

(1. Xidian University, Xi'an 710000, China;  
2. ZTE Corporation, Shenzhen 518057, China)

DOI: 10.12142/ZTECOM.202304011

<https://kns.cnki.net/kcms/detail/34.1294.TN.20231107.1357.002.html>,  
published online November 8, 2023

Manuscript received: 2023-04-28

**Abstract:** This paper proposes a design and fine-tuning method for mixed electric and magnetic coupling filters. It derives the quantitative relationship between the coupling coefficients (electric and magnetic coupling, i. e.,  $E_c$  and  $M_c$ ) and the linear coefficients of frequency-dependent coupling for the first time. Different from the parameter extraction technique using the bandpass circuit model, the proposed approach explicitly relates  $E_c$  and  $M_c$  to the coupling matrix model. This paper provides a general theoretic framework for computer-aided design and tuning of a mixed electric and magnetic coupling filter based on coupling matrices. An example of a 7th-order coaxial combline filter design is given in the paper, verifying the practical value of the approach.

**Keywords:** coupling matrix; frequency-dependent coupling; mixed electric and magnetic coupling; parameter extraction

**Citation** (Format 1): XIONG Z A, ZHAO P, FAN J Y, et al. Mixed electric and magnetic coupling design based on coupling matrix extraction [J]. *ZTE Communications*, 2023, 21(4): 85 – 90. DOI: 10.12142/ZTECOM.202304011

**Citation** (Format 2): Z. A. Xiong, P. Zhao, J. Y. Fan, et al., “Mixed electric and magnetic coupling design based on coupling matrix extraction,” *ZTE Communications*, vol. 21, no. 4, pp. 85 – 90, Dec. 2023. doi: 10.12142/ZTECOM.202304011.

## 1 Introduction

In the design of microwave filters, the realization of finite transmission zeros (TZs) is critical to improving selectivity. Cross-coupling is the most popular method to create TZs<sup>[1]</sup>. However, this multi-path mechanism often leads to complexity in the design of filter layout, especially for high-order filters with many TZs. To solve this problem, frequency-dependent coupling (FDC) is introduced into the filter design. In an FDC, the coupling coefficient will be zero at a specific frequency, creating extra TZs in a given filter network.

SZYDLOWSKI et al.<sup>[2-5]</sup> proposed an optimization-based approach to the synthesis of coupling matrices with FDCs. Years later, HE<sup>[6-7]</sup> and ZHAO<sup>[8]</sup> developed deterministic matrix transformation approaches that can eliminate one cross-coupling from traditional  $N$ -tuples and introduce FDCs into the network. Constant couplings can be realized as pure electric or magnetic coupling, whereas FDCs need to be implemented as mixed electric and magnetic couplings. However, the mixed electric and magnetic coupling is difficult to control, because there is no quantitative relationship between FDCs and the mixed electric and magnetic couplings.

In 2006, MA<sup>[9]</sup> proposed constructing an electrical coupling

and a magnetic coupling path between two resonators to generate a TZ. However, he did not give the relationship between the TZ position and the electric and magnetic coupling coefficients. In 2008, CHU<sup>[10-11]</sup> defined the mixed electric and magnetic coupling coefficient and gave the extraction method of the electric coupling coefficient ( $E_c$ ) and the magnetic coupling coefficient ( $M_c$ ) from the electromagnetic (EM) simulation of mixed electric and magnetic coupling structures. Furthermore, the relationship between the location of TZ and ( $E_c$ ,  $M_c$ ) is found. However, the parameter extraction is carried out in the bandpass domain. The approach does not explicitly relate  $E_c$  and  $M_c$  to the coupling matrix model, which is popular in filter synthesis. Therefore, it is difficult to design or tune the mixed coupling by coupling matrix extraction approaches.

This paper derives the explicit relationship between  $E_c$  ( $M_c$ ) in the mixed electric and magnetic coupling and elements in the coupling and capacitance matrices. With the coupling matrix extracted by the model-based vector fitting (MVF) technique<sup>[12]</sup>, the filter designer can easily design and tune the mixed coupling filter by comparing the extracted matrices with target ones.

The rest of the paper is organized as follows. Section 2 derives the relationship between the lowpass FDC model and the bandpass mixed coupling coefficients ( $E_c$  and  $M_c$ ). Section 3 presents a mixed electric and magnetic coupling physical

This work was supported by the National Natural Science Foundation of China under Grant No. 62001339.

model. The theory proposed in Section 2 is applied to design the mixed coupling structure. We then demonstrate a 7th-order in-line mixed coupling filter design with the aid of coupling matrix extraction. Section 4 concludes this paper.

## 2 Relationship Between FDC and Mixed Electric and Magnetic Coupling

A constant coupling in the coupling matrix is modeled by an ideal J-inverter, the  $\pi$ -equivalent circuit of which consists of three frequency-invariant susceptances (FISs). The characteristic admittance of a frequency-dependent inverter varies with frequency. Fig. 1 shows the  $\pi$ -equivalent circuit model of the frequency-dependent inverter. The circuit model includes three capacitors parallel-connected with FISs.

Note that the FDC is an element in lowpass circuit models. The bandpass frequency is mapped to the lowpass frequency domain by:

$$\Omega = \frac{\omega_0}{\omega_2 - \omega_1} \left( \frac{\omega}{\omega_0} - \frac{\omega_0}{\omega} \right), \quad (1)$$

where  $\Omega$  is the normalized lowpass frequency,  $\omega_0$  is the center frequency of the bandpass filter,  $\omega_2$  is the upper band edge frequency,  $\omega_1$  is the lower band edge, and  $\omega$  is the bandpass frequency.

Substituting Eq. (1) into the admittance formula of FIS and capacitor connected in parallel yields

$$Y = jB + j \frac{\omega_0}{\omega_2 - \omega_1} \left( \frac{\omega}{\omega_0} - \frac{\omega_0}{\omega} \right) C_{LP} = jB + j\omega C_{BP} + \frac{1}{j\omega L_{BP}}, \quad (2)$$

where  $C_{LP}$  is the capacitance in the lowpass circuit model,  $C_{BP}$  is the capacitance, and  $L_{BP}$  is the inductance in the bandpass circuit model. According to Eq. (2), the parameters in the lowpass and bandpass circuits are related by:

$$C_{BP} = \frac{C_{LP}}{2\pi BW}, \quad L_{BP} = \frac{2\pi BW}{\omega_0^2 C_{LP}}, \quad (3)$$

where  $BW$  is the bandwidth and  $2\pi BW = \omega_2 - \omega_1$ . After transformation, the coupling between two resonators is not a pure electric or magnetic coupling form but mixed coupling. Therefore, an FDC should be realized as a mixed electric and magnetic coupling. However, Eq. (3) cannot reveal the qualitative relationship between FDC and mixed electric and magnetic coupling.

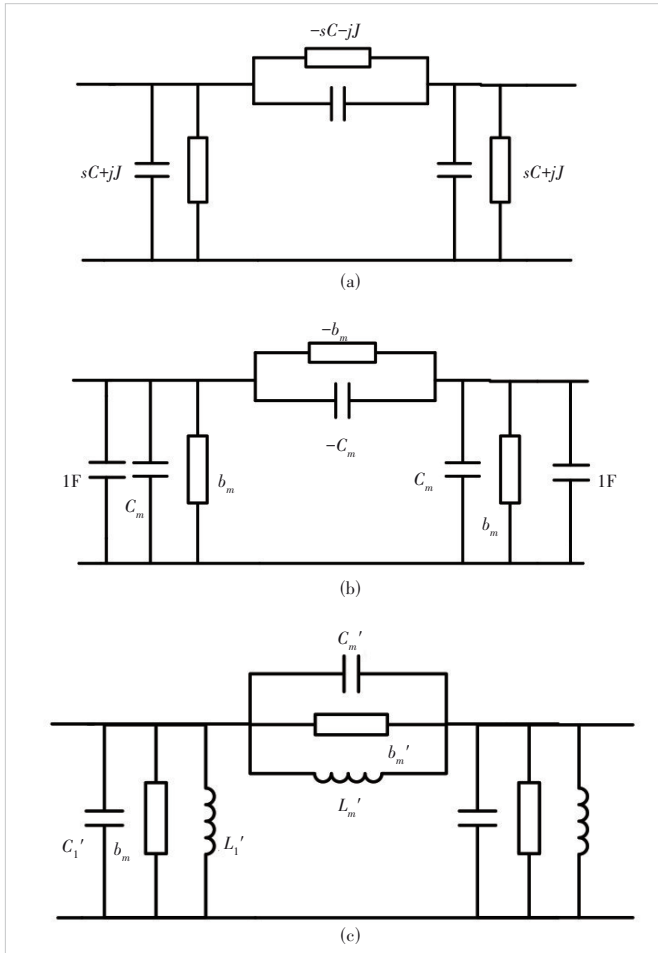
As shown in Fig. 1(b), there are unity capacitors on both sides of the frequency-dependent inverter. The capacitors model parallel resonant circuits with a resonant frequency of zero rad/s. The value of the frequency-dependent inverter is  $sC_m + jb_m$ . If the left node index is  $i$  and the right node index is  $j$ , the coupling matrix element  $M_{ij}$  is  $b_m$ , and the capacitance matrix element  $C_{ij}$  is  $C_m$ . After lowpass-to-bandpass circuit transformation in Eq. (3), the resultant bandpass circuit model is shown in Fig. 1(c), where

$$C_1' = \frac{1 + C_m}{2\pi BW}, \quad C_m' = -\frac{C_m}{2\pi BW}, \quad (4a)$$

$$L_1' = \frac{2\pi BW}{\omega_0^2(1 + C_m)}, \quad L_m' = -\frac{2\pi BW}{\omega_0^2 C_m}, \quad (4b)$$

$$b_m' = -b_m, \quad (4c)$$

$$\omega_m \approx \omega_0 - \frac{b_m \pi BW}{C_m}. \quad (4d)$$



▲ Figure 1.  $\pi$ -equivalent circuit model: (a) frequency-dependent inverter, where the admittances of capacitance and frequency-invariant susceptances are  $sC(-sC)$  and  $jJ(-jJ)$  respectively; (b) frequency-dependent inverter coupled lowpass network consisting of two resonators, where the two resonators are unit capacitors and resonant frequency is zero rad/s; (c) bandpass circuit model of mixed electric and magnetic coupling

In the above derivation, we use the narrowband condition of  $\omega_0 \gg BW$ . This condition also applies to the derivation of Eqs. (7), (9) and (10).  $\omega_m$  is the resonant frequency. When the frequency is  $\omega_m$ , the parallel  $C_m'$ ,  $L_m'$  and  $b_m'$  form an open circuit, and the signal transmission is blocked to generate a TZ.

For a mixed electric and magnetic coupling, the calculation formula of  $E_C$  and  $M_C$  can be expressed as follows<sup>[10]</sup>:

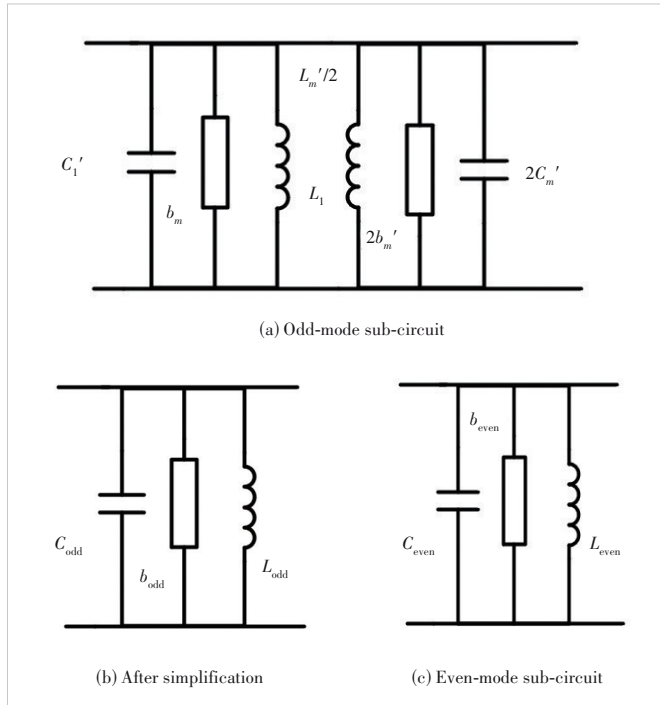
$$E_C = \frac{\omega_{ev}^2 - \omega_{od}^2}{\omega_{ev}^2 + \omega_{od}^2 - 2\omega_m^2}, \quad (5a)$$

$$M_C = \frac{\omega_m^2(\omega_{ev}^2 - \omega_{od}^2)}{2\omega_{ev}^2\omega_{od}^2 - \omega_m^2(\omega_{ev}^2 + \omega_{od}^2)^2}, \quad (5b)$$

where  $\omega_{ev}$  is the even mode resonant frequency, and  $\omega_{od}$  is the odd mode resonant frequency of a coupled resonator pair.

We can calculate  $E_C$  and  $M_C$  in the mixed electric and magnetic coupling based on  $\omega_m$ ,  $\omega_{ev}$ , and  $\omega_{od}$ . To obtain  $E_C$  and  $M_C$  of the mixed electric and magnetic coupling in terms of FDC coefficients, we can analyze the even- and odd-mode resonant frequencies of the coupled-resonator circuit model in Fig. 1(c).

We analyze the odd mode first. The odd-mode sub-circuit is shown in Fig. 2(a). After combining parallel-connected capacitors, inductors, and FISs, the odd-mode sub-circuit is transformed into the form shown in Fig. 2(b). We have:



▲ Figure 2. Mode circuit of a bandpass circuit model of mixed electric and magnetic coupling

$$C_{\text{odd}} = C_1' - 2C_m' = \frac{1 - C_m}{2\pi BW}, \quad (6a)$$

$$L_{\text{odd}} = \frac{2C_1'C_m'}{C_1' + 2C_m'} = \frac{2\pi BW}{\omega_0^2 - \omega_0^2 C_m}, \quad (6b)$$

$$b_{\text{odd}} = -b_m. \quad (6c)$$

Therefore, the resonant frequency of the odd mode is

$$\omega_{\text{od}} = \sqrt{\frac{b_{\text{odd}}^2 + 4\frac{C_{\text{odd}}}{L_{\text{odd}}} - b_{\text{odd}}}{2C_{\text{odd}}}} \approx \omega_0 + \frac{b_m \pi BW}{1 - C_m}. \quad (7)$$

Similarly, to analyze the even mode, as shown in Fig. 2(c), we have

$$C_{\text{even}} = \frac{1 + C_m}{2\pi BW}, \quad (8a)$$

$$L_{\text{even}} = \frac{2\pi BW}{\omega_0^2(1 + C_m)}, \quad (8b)$$

$$b_{\text{even}} = b_m. \quad (8c)$$

Therefore, the resonant frequency of the even mode sub-circuit is

$$\omega_{\text{even}} = \sqrt{\frac{b_{\text{even}}^2 + 4\frac{C_{\text{even}}}{L_{\text{even}}} - b_{\text{even}}}{2C_{\text{even}}}} \approx \omega_0 - \frac{b_m \pi BW}{1 + C_m}. \quad (9)$$

Substituting Eqs. (7) and (9) into Eq. (5) yields

$$E_C = \frac{\omega_{ev}^2 - \omega_{od}^2}{\omega_{ev}^2 + \omega_{od}^2 - 2\omega_m^2} \approx -C_m, \quad (10a)$$

$$M_C = \frac{\omega_m^2(\omega_{ev}^2 - \omega_{od}^2)}{2\omega_{ev}^2\omega_{od}^2 - \omega_m^2(\omega_{ev}^2 + \omega_{od}^2)^2} \approx -C_m. \quad (10b)$$

The results in Eq. (10) show that  $E_C$  and  $M_C$  in mixed electric and magnetic coupling filters are almost equal, and both values are approximately equal to  $-C_m$ . This analysis result reveals that the majority of electric and magnetic coupling should be canceled with each other to realize an FDC. The

electric coupling or magnetic coupling is slightly stronger than the other one to provide a weak total coupling for constructing the narrowband passband. Therefore, if the absolute value of the synthesized capacitance matrix element  $C_{ij}$  is larger, the electric and magnetic coupling in the mixed coupling structure should be tuned stronger simultaneously.

To conclude, the FDC in the lowpass coupling matrix model is  $sC_{ij} + jM_{ij}$ , where  $M_{ij}$  represents the total coupling exhibited by the mixed electric and magnetic coupling at the center frequency, and  $C_m$  is related to the strength of both the electric and the magnetic coupling coefficient in the mixed coupling.

### 3 Analysis of Electromagnetic Model

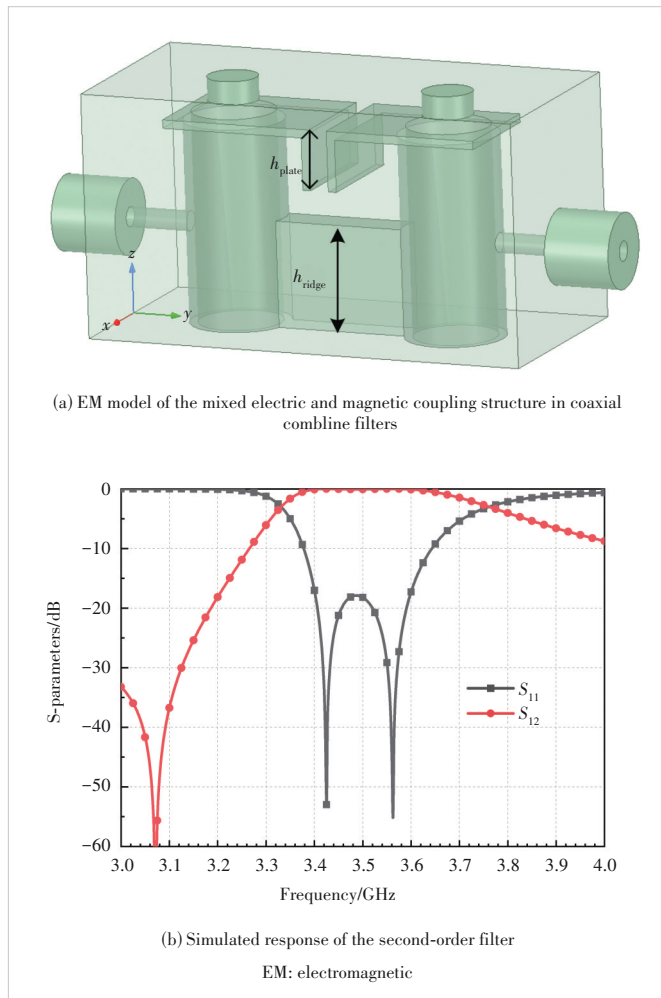
For the experimental validation, a 7th-order in-line bandpass filter is designed with coaxial cavity structures in this section. The 7th-order filter contains two mixed electric and magnetic couplings, the structure of which is shown in Fig. 3(a). The simulation results of the second-order filter block are shown in Fig. 3(b). The center frequency of the filter is 3.5 GHz, and the bandwidth is 0.2 GHz, and the return loss is 18 dB. The open

end of the metal rod is connected to a folded metal sheet. Two adjacent metal sheets form a parallel plate capacitor to realize a strong electric coupling. The height of the plate  $h_{plate}$  is 3.6 mm. The short ends of adjacent coaxial resonators are connected by a metal ridge to realize a strong magnetic coupling. The height of the ridge,  $h_{ridge}$ , is 6.3 mm. The strong electrical coupling and the magnetic coupling exist simultaneously to form a mixed electric and magnetic coupling. If  $h_{plate}$  or  $h_{ridge}$  increases, the electric coupling or magnetic coupling will become stronger in this design.

By repeatedly applying the MVF technique to extract the coupling matrix from simulation data<sup>[12]</sup>, we can study the relationship between the mixed coupling coefficients and the element values of the coupling and capacitance matrices. Tables 1 and 2 show the extracted values of  $M_{ij}$  and  $C_{ij}$  when  $E_C$  and  $M_C$  are changed. It can be found from Table 1 that when  $h_{ridge}$  and  $h_{plate}$  increase simultaneously,  $C_{ij}$  increases, whereas  $M_{ij}$  almost does not change. Therefore,  $C_{ij}$  is related to both the electric and magnetic coupling coefficients in the mixed coupling.

Table 2 shows that when  $E_C$  increases and  $M_C$  decreases,  $M_{ij}$  increases. Since  $M_{ij}$  represents the total coupling exhibited by the mixed electric and magnetic coupling at the center frequency, it can be seen that  $E_C$  is stronger than  $M_C$  in the mixed coupling structure shown in Fig. 3(a). Table 2 also shows that we can control  $M_{ij}$  by increasing the difference between  $E_C$  and  $M_C$  without affecting  $C_{ij}$ .

Table 3 shows that when  $M_C$  increases, the TZ is shifted to



▲ Figure 3. EM model and response of second-order filter

▼ Table 1. Simultaneously changing the heights of the ridge and the plate

$h_{ridge}/mm$	$h_{plate}/mm$	$M_{ij}$	$C_{ij}$	TZ/rad
6.70	3.96	1.436 2	0.369 5	-3.89
6.50	3.78	1.440 9	0.355 3	-4.06
6.30	3.60	1.440 2	0.343 3	-4.20
6.10	3.43	1.443 8	0.331 8	-4.35
5.90	3.27	1.438 3	0.320 9	-4.48

TZ: transmission zero

▼ Table 2. Changing the height of the ridge or the plate

$h_{ridge}/mm$	$h_{plate}/mm$	$M_{ij}$	$C_{ij}$	TZ/rad
6.70	3.43	0.794 5	0.341 8	-2.32
6.50	3.50	1.097 2	0.341 8	-3.21
6.30	3.60	1.440 2	0.343 3	-4.20
6.10	3.68	1.761 0	0.343 7	-5.12
5.90	3.75	2.056 8	0.343 8	-5.98

TZ: transmission zero

▼ Table 3. Changing the height of the ridge or the plate when TZ is in the lower stopband

$h_{ridge}/mm$	$h_{plate}/mm$	$M_{ij}$	$C_{ij}$	TZ/rad
6.30	3.60	1.440 2	0.343 3	-4.20
6.90	3.60	0.760 1	0.353 5	-2.15
7.50	3.60	-0.029 4	0.363 0	0.08
8.10	3.60	-0.912 7	0.372 8	2.45
8.70	3.60	-1.601 0	0.397 9	4.02

TZ: transmission zero

the right. From Table 4, it can be found that when  $E_C$  increases, the TZ is shifted to the left. From Tables 3 and 4, we can also see that when the TZ is located in the lower stopband,  $E_C$  is stronger than  $M_C$ . If the TZ is in the upper stopband, then  $M_C$  is stronger than  $E_C$ .

To conclude, the tuning of the mixed electric and magnetic coupling structure in Fig. 3(a) follows two rules:

Rule 1: We simultaneously increase or decrease  $E_C$  and  $M_C$  to tune  $C_{ij}$ .

Rule 2: If the TZ is in the lower stopband, we can increase  $E_C$  and decrease  $M_C$  to increase  $M_{ij}$ . If the TZ is in the upper stopband, we can increase  $M_C$  and decrease  $E_C$  simultaneously to increase  $M_{ij}$ .

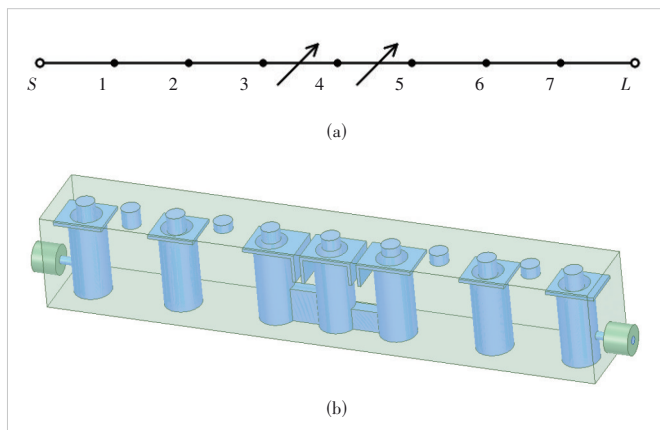
To verify the above theory, take a 7th-order filter with the coupling topology shown in Fig. 4(a) as an example. The center frequency and bandwidth of the filter are 3.5 GHz and 200 MHz, respectively. The in-band return loss level is required to be 18 dB. Two TZs at 3.7 GHz and 3.3 GHz are generated sequentially by two mainline FDCs. The synthesized coupling matrix and capacitance matrix are shown in Figs. 5 and 6, respectively.

The perspective view of the filter model is shown in Fig. 4(b). With the help of the MVF method to extract the coupling matrix from simulation data, we can identify how to adjust the dimensions and finally obtain satisfactory filter responses. The simulation results with ideal lossless materials are shown in Fig. 7, where solid lines are simulation data, and dashed lines are the

▼ Table 4. Changing the height of the ridge or the plate when TZ is in the upper stopband

$h_{\text{ridge}}/\text{mm}$	$h_{\text{plate}}/\text{mm}$	$M_{ij}$	$C_{ij}$	TZ/rad
6.30	1.60	-0.958 2	0.236 2	4.06
6.30	2.10	-0.376 8	0.265 4	1.42
6.30	2.60	0.212 7	0.293 0	-0.73
6.30	3.10	0.822 3	0.318 9	-2.58
6.30	3.60	1.440 2	0.343 3	-4.20

TZ: transmission zero



▲ Figure 4. 7th-order filter with mixed electric and magnetic coupling: (a) target topology and (b) electromagnetic model of the 7th-order filter with mixed electric and magnetic coupling

ideal synthesis responses.

## 4 Conclusions

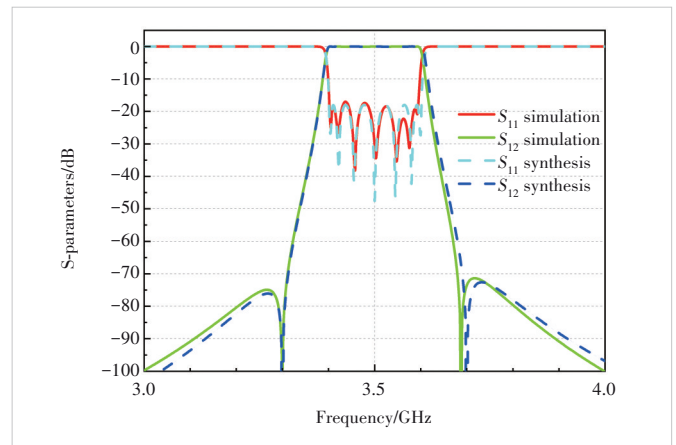
In this paper, the relationship between the coupling matrix (capacitance matrix) and  $E_C$  ( $M_C$ ) is obtained through circuit analysis. A filter example is designed to verify the proposed theory. Although only the inline filter is discussed in detail, the strategy introduced in this paper can be easily generalized to mixed electric and magnetic coupling filters in different coupling topologies. Compared with the existing theory of mixed electric and magnetic coupling filters, this work has the following distinctive features.

0	0.952 2	0	0	0	0	0	0	0
0.952 2	0.000 4	0.793 8	0	0	0	0	0	0
0	0.793 8	0.000 5	0.555 8	0	0	0	0	0
0	0	0.555 8	0.342 2	0.580 9	0	0	0	0
0	0	0	0.580 9	0.023 1	0.571 4	0	0	0
0	0	0	0	0.571 4	0.321 4	0.559 5	0	0
0	0	0	0	0	0.559 5	0.000 5	0.793 8	0
0	0	0	0	0	0	0.793 8	0.000 4	0.952 2
0	0	0	0	0	0	0	0.952 2	0

▲ Figure 5. Coupling matrix

0	0	0	0	0	0	0	0	0
0	1	0	0	0	0	0	0	0
0	0	1	0	0	0	0	0	0
0	0	0	1	-0.298 5	0	0	0	0
0	0	0	-0.298 5	1	0.277 3	0	0	0
0	0	0	0	0.277 3	1	0	0	0
0	0	0	0	0	0	1	0	0
0	0	0	0	0	0	0	1	0
0	0	0	0	0	0	0	0	1

▲ Figure 6. Capacitance matrix



▲ Figure 7. Response of the 7th-order, where dashed lines are ideal synthesis responses and solid lines are simulation results

1) It derives the explicit relationship between  $E_c(Mc)$  in the mixed electric and magnetic coupling and elements in the coupling and capacitance matrices.

2) The filter tuning procedure is based on analytical coupling matrix extraction and thus is very fast, compared with optimization-based filter tuning techniques.

This paper gives a guiding idea for designing the physical model of the mixed electric and magnetic coupling filter.

## References

- [1] CAMERON R J, KUDSIA C M, MANSOUR R R. Microwave filters for communication systems [M]. New York, USA: Wiley, 2018. DOI: 10.1002/9781119292371
- [2] SZYDŁOWSKI L, LAMECKI A, MROZOWSKI M. Coupled-resonator waveguide filter in quadruplet topology with frequency-dependent coupling - A design based on coupling matrix [J]. IEEE microwave and wireless components letters, 2012, 22(11): 553 - 555. DOI: 10.1109/LMWC.2012.2225604
- [3] SZYDŁOWSKI L, LESZCZYŃSKA N, LAMECKI A, et al. A substrate integrated waveguide (SIW) bandpass filter in a box configuration with frequency-dependent coupling [J]. IEEE microwave and wireless components letters, 2012, 22(11): 556 - 558. DOI: 10.1109/LMWC.2012.2221690
- [4] SZYDŁOWSKI L, MROZOWSKI M. A self-equalized waveguide filter with frequency-dependent (resonant) couplings [J]. IEEE microwave and wireless components letters, 2014, 24(11): 769 - 771. DOI: 10.1109/LMWC.2014.2303171
- [5] SZYDŁOWSKI L, LESZCZYŃSKA N, LAMECKI A, et al. A substrate integrated waveguide (SIW) bandpass filter in A box configuration with frequency-dependent coupling [J]. IEEE microwave and wireless components letters, 2012, 22(11): 556 - 558. DOI: 10.1109/LMWC.2012.2221690
- [6] HE Y X, MACCHIARELLA G, WANG G, et al. A direct matrix synthesis for in-line filters with transmission zeros generated by frequency-variant couplings [J]. IEEE transactions on microwave theory and techniques, 2018, 66(4): 1780 - 1789. DOI: 10.1109/tmtt.2018.2791940
- [7] HE Y X, WANG G, SUN L G, et al. Direct matrix synthesis for in-line filters with transmission zeros generated by frequency-variant couplings [C]/IEEE MTT-S International Microwave Symposium (IMS). IEEE, 2017: 356 - 359. DOI: 10.1109/MWSYM.2017.8059119
- [8] ZHAO P, WU K. Cascading fundamental building blocks with frequency-dependent couplings in microwave filters [J]. IEEE transactions on microwave theory and techniques, 2019, 67(4): 1432 - 1440. DOI: 10.1109/TMTT.2019.2895532
- [9] MA K X, MA J G, YEO K S, et al. A compact size coupling controllable filter with separate electric and magnetic coupling paths [J]. IEEE transactions on microwave theory and techniques, 2006, 54(3): 1113 - 1119. DOI: 10.1109/TMTT.2005.864118
- [10] CHU Q X, WANG H. An inline coaxial quasi-elliptic filter with controllable mixed electric and magnetic coupling [J]. IEEE transactions on microwave theory and techniques, 2009, 57(3): 667 - 673. DOI: 10.1109/TMTT.2009.2013290
- [11] CHU Q X, WANG H. A compact open-loop filter with mixed electric and magnetic coupling [J]. IEEE transactions on microwave theory and techniques, 2008, 56(2): 431 - 439. DOI: 10.1109/TMTT.2007.914642
- [12] ZHAO P, WU K L. Model-based vector-fitting method for circuit model extraction of coupled-resonator diplexers [J]. IEEE transactions on microwave theory and techniques, 2016, 64(6): 1787 - 1797. DOI: 10.1109/TMTT.2016.2558639

## Biographies

**XIONG Zhiang** received his BS degree from Jiangxi University of Science and Technology, China in 2021. He is currently pursuing his master's degree in electromagnetic wave and microwave technology at Xidian University, China. His current research interests include mixed electric and magnetic coupling filter, and modeling and optimization of microwave passive filters.

**ZHAO Ping** (aoing56@gmail.com) received his BS degree from Nanjing University, China, in 2012, and PhD degree from The Chinese University of Hong Kong, China in 2017. From 2017 to 2019, he was a post-doctoral researcher with the École Polytechnique de Montréal, Canada. In 2020, he joined the National Key Laboratory of Antennas and Microwave Technology, School of Electronic Engineering, Xidian University, China, as an associate professor. His research interests include coupling matrix synthesis techniques for coupled-resonator networks, analytical computer-aided tuning (CAT) algorithms for microwave and millimeter-wave filters, and diplexers with applications in cellular base stations and satellites. He is also interested in modeling and optimization of passive RF components and computer-aided design techniques, such as the homotopy method, artificial neural networks, and machine learning techniques. He is a member of IEEE.

**FAN Jiyuan** received his BS degree from the Nanjing University of Posts and Telecommunications, China in 2022. He is currently pursuing the master's degree in electro-magnetic wave and microwave technology at Xidian University, China.

**WU Zengqiang** received his master's degree from Xidian University, China in 2018. The same year, he joined ZTE Corporation as an assistant engineer. His current research interests include miniaturization techniques and lossless techniques of microwave filters for wireless communication, such as coaxial filter and dielectric waveguide filter.

**Gong Hongwei** joined ZTE Corporation as a senior engineer. His current research interests include miniaturization techniques and lossless techniques of microwave filters for wireless communication, such as the coaxial filter and the dielectric waveguide filter.